Surface brightens-up Si quantum dots: direct bandgap-like size-tunable emission

Dohnalová, K.; Poddubny, A. N.; Prokofiev, A.A.; de Boer, W.D.A.M.; Umesh, C.P.; Paulusse, J.M.J.; Zuilhof, H.; Gregorkiewicz, T.

DOI
10.1038/lsa.2013.3

Publication date
2013

Document Version
Final published version

Published in
Light: Science & Applications

Light: Science & Applications (2013) 2, e47; doi:10.1038/lsa.2013.3

www.nature.com/lsa

ORIGINAL ARTICLE

Surface brightens up Si quantum dots: direct bandgap-like size-tunable emission

Kateřina Dohnalová[1], Alexander N Poddubny[1,4], Alexei A Prokofiev[1,4], Wieteke DAM de Boer[1], Chinnaswamy P Umesh[2], Jos MJ Paulusse[2,5], Han Zuilhof[2,3] and Tom Gregorkiewicz[1]

Colloidal semiconductor quantum dots (QDs) constitute a perfect material for ink-jet printable large area displays, photovoltaics, light-emitting diode, bio-imaging luminescent markers and many other applications. For this purpose, efficient light emission/absorption and spectral tunability are necessary conditions. These are currently fulfilled by the direct bandgap materials. Si-QDs could offer the solution to major hurdles posed by these materials, namely, toxicity (e.g., Cd-, Pb- or As-based QDs), scarcity (e.g., QD with In, Se, Te) and/or instability. Here we show that by combining quantum confinement with dedicated surface engineering, the biggest drawback of Si—the indirect bandgap nature—can be overcome, and a 'direct bandgap' variety of Si-QDs is created. We demonstrate this transformation on chemically synthesized Si-QDs using state-of-the-art optical spectroscopy and theoretical modelling. The carbon surface termination gives rise to drastic modification in electron and hole wavefunctions and radiative transitions between the lowest excited states of electron and hole attain 'direct bandgap-like' (phonon-less) character. This results in efficient fast emission, tunable within the visible spectral range by QD size. These findings are fully justified within a tight-binding theoretical model. When the C surface termination is replaced by oxygen, the emission is converted into the well-known red luminescence, with microsecond decay and limited spectral tunability. In that way, the 'direct bandgap' Si-QDs convert into the 'traditional' indirect bandgap form, thoroughly investigated in the past.
Light: Science & Applications (2013) **2,** e47; doi:10.1038/lsa.2013.3; published online 4 January 2013

Keywords: direct bandgap; optical spectroscopy; optoelectronics; organic capping; silicon quantum dots; tight binding model

INTRODUCTION

Compared to brightly emitting organic molecules, which are presently used in a wide variety of applications, quantum dots (QDs) are more robust, have larger absorption cross-sections and their emission wavelength can be tuned by size, and thus offer optical and chemical advantages. Silicon, being non-toxic and abundant, eliminates most of the drawbacks commonly found for the direct bandgap materials, and therefore provides an excellent benign and cheap solution for these issues. One major drawback—the indirect bandgap, and therefore, low probability of radiative recombination (radiative rate), is only partially overcome in Si-QDs by quantum confinement.[1–4] The most frequently investigated Si-QD systems are H-terminated, with wide spectral tunability but chemically instable and prone to oxidation,[5–7] and O-terminated, with excellent optical and chemical stability, but limited tunability and low radiative rates ($k_{rad}=10^4$–10^6 s^{-1}).[2,3] More versatile surface engineering and customisable organic termination can be achieved by chemical synthesis,[8–11] which also could allow for macroscopic production yields of Si-QDs.[12] In this case, alkyl-chains are good candidates for surface passivation, stabilizing it, preventing photo-oxidation (owing to formation of a strong covalent Si–C bond), and averting aggregation in solution.[8] In the past, optical investigations of chemically synthesized Si-QDs have revealed nanosecond emission tunable in the visible.[12–16] However, the microscopic origin of this emission has been a matter of debate due to: (i) diversity of results obtained by different groups (see, e.g., the introductory remarks in Ref. 11); (ii) the fact that emission characteristics of many organic solvents and compounds used for, or being produced, in the synthesis are very similar to the presumed Si-QD emission;[17,18] (iii) difficulties to assess the size effects on optical properties due to lack of techniques for synthesis of batches with well-defined sizes; (iv) lack of theoretical models for larger organically terminated Si-QDs that could correlate size and surface effects with the observed fast emission rates and emission spectra (ab-initio calculations being available only for ultra-small alkyl-terminated nanoclusters with $d_{QD}<1.5$ nm).[19]

In this work, we present results of optical spectroscopy investigations of chemically synthesized alkyl-capped Si-QDs. These Si-QDs show photoluminescence (PL) tunable in the visible range with nanosecond decay. By thorough analysis, we provide conclusive evidence that this very characteristic emission originates from no-phonon radiative recombination of electron-hole pairs (excitons) confined in

[1]Van der Waals-Zeeman Institute, University of Amsterdam, NL-1098 XH Amsterdam, The Netherlands; [2]Laboratory of Organic Chemistry, Wageningen University, 6703 HB Wageningen, The Netherlands; [3]Department of Chemical and Materials Engineering, King Abdulaziz University, Jeddah, Saudi Arabia; [4]Ioffe Physical-Technical Institute RAS, 26 Polytechnicheskaya, 194021 Saint-Petersburg, Russia and [5]Current address: MIRA Institute, Department of Biomedical Chemistry, University of Twente, Building Zuidhorst Enschede, The Netherlands
Correspondence: Dr K Dohnalová, Van der Waals-Zeeman Institute, University of Amsterdam, Science Park 904, NL-1098 XH Amsterdam, The Netherlands
E-mail: k.dohnalova@uva.nl
Received 5 July 2012; revised 11 September 2012; accepted 25 September 2012

the core of Si-QDs. In order to justify this identification, the optical properties of C-terminated Si-QDs are modelled within an $sp^3d^5s^*$ empirical tight binding approximation. We show that the carbon layer at the surface modifies electron and hole wavefunctions, dramatically increasing the radiative rate of no-phonon recombination to the level characteristic for direct bandgap materials. In order to conclusively confirm the proposed identification, and also to explore the possibility of influencing QD emission by surface termination, we explicitly demonstrate that upon oxidation, the observed fast blue PL transforms into the well-known, slowly decaying red emission band, in a similar way as demonstrated in the past for H-terminated Si-QDs.[5] This transformation complements and also validates earlier demonstrations that replacement of O-termination of the Si-QD surface by alkyl groups blue-shifts the slow red emission and enhances its rate.[20] In that way, we convincingly demonstrate that Si-QDs constitute a viable, truly benign and environmentally friendly replacement for the currently considered heavy metal (Cd, Pb) QDs, with no compromise to optical properties. On the fundamental side, the current finding proves that in semiconductor QDs, both the energy and the structure of the bandgap can be effectively manipulated.

MATERIALS AND METHODS

Si-QDs were prepared *via* a wet-chemical method[10] adapted from Kauzlarich and co-workers.[21] Magnesium silicide (Mg_2Si) was oxidized with bromine (Br_2) in refluxing n-octane during 3 days. Formed bromine-terminated Si-QDs were passivated using n-butyllithium, resulting in n-butyl-terminated Si-QDs. The main side product, bromo-octane, and other impurities, were removed using silica column chromatography, yielding approximately 50 mg of a brown/orange, waxy material. Butyl-terminated Si-QDs are photostable and freestanding. This type of synthesis produces typically Si-QDs with average diameter of $d_{QD}=2.2\pm0.5$ nm. For spectral analysis, the Si-QDs are dispersed in ultraviolet grade ethanol. Further details on the sample material preparation and characterisation can be found in Ref. 10 and Supplementary Information.

PL emission spectra in Figures 1 and 2 have been measured using thermoelectric-cooled charge-coupled device (Hamamatsu) coupled to an imaging spectrometer (M266, Solar Laser Systems). For excitation, we used Xe lamp (150 W, Hamamatsu; Figure 1c) and ns-pulsed laser (OPO system pumped by Nd:YAG, 7 ns pulse duration, repetition rate 100 Hz; Figures 1a and 2a). The PL lifetime (Figures 1b and 2b) was measured using aforementioned ns-laser pulsed excitation and fs-laser pulsed excitation (Ti-sapphire laser pumped Optical Parametric Amplifier, 370 nm, 140 fs pulse duration, repetition rate of 4 MHz). Signal was detected by PMT (Hamamatsu) in a time-correlated photon-counting regime (instrumental response time of 26 ps). All measurements were done at room temperature and spectra are corrected for spectral sensitivity of the detection system.

RESULTS AND DISCUSSIONS

The absorption and emission characteristics of the synthesized QDs are shown in Figure 1. Figure 1a displays different colours of PL obtained upon different excitation energies, with the corresponding PL spectra shown in Figure 1c. Figure 1b shows characteristic fast PL

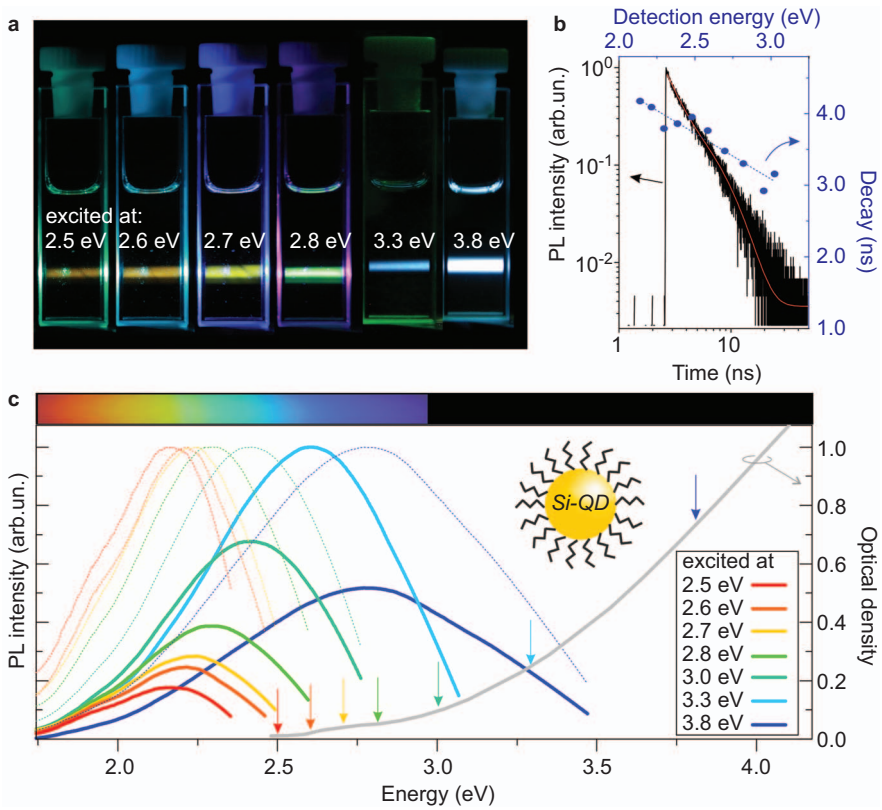

Figure 1 Tunable PL of butyl-terminated Si-QDs. (**a**) Real colour photos of Si-QDs upon different excitations, indicated in the photo and in (**c**) also by coloured arrows. (**b**) Fast ~4 ns PL lifetime detected at ~2.6 eV (black, left vertical axis) and spectral dependence of PL decays (blue, right vertical axis). (**c**) The corresponding PL spectra of the Si-QDs (left vertical axis) plotted together with optical density (right vertical axis). The PL spectra are corrected for response of detection, excitation intensity and absorption at each particular wavelength (thick colour lines) and normalized (thin dotted colour lines). PL, photoluminescence; QD, quantum dot.

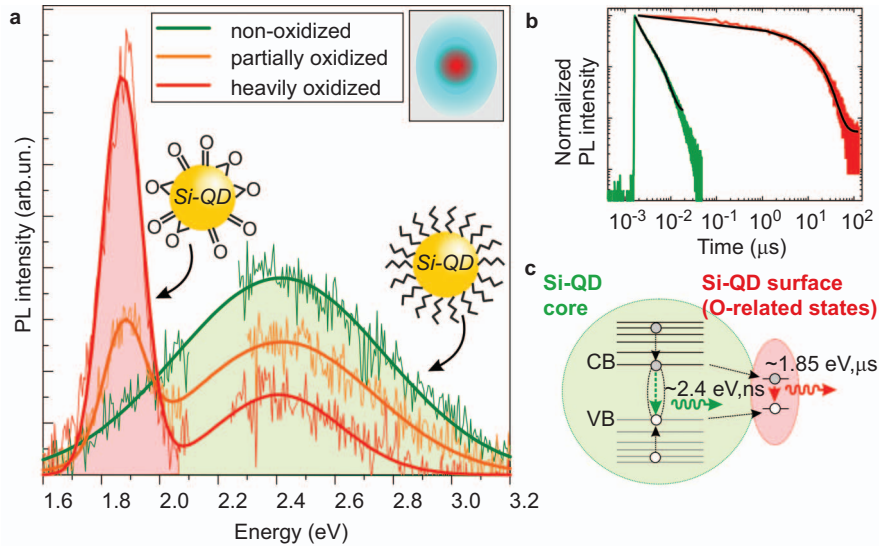

Figure 2 PL from C- and O-terminated Si-QDs. (**a**) PL spectra of C-terminated (green), partially oxidized (orange) and heavily oxidized (red) Si-QDs. The oxidized sample shows two contributions around 1.85 and 2.4 eV, whereas the C-terminated shows only the latter band. The inset shows a sketch of the optically excited spot (blue) and the photo-oxidized area (red). (**b**) PL dynamics recorded at 1.85 eV (red) with decay $\tau_{PL}\approx12$ μs and at 2.4 eV with decay of $\tau_{PL}\approx4$ ns. (**c**) Schematic illustration of carrier recombination processes giving rise to the microsecond decaying PL band around 1.85 eV, and the nanosecond decaying band centred at 2.4 eV. The former is related to carriers trapped at an O-related defect state at the surface of the QD, while the latter corresponds to the QD core-related recombination. PL, photoluminescence; QD, quantum dot.

dynamics, detected at ~2.6 eV (black), and spectral dependence of PL decays (blue). The PL spectra in Figure 1c feature a broad band, with its maximum intensity shifting from ~2.75 eV for the highest photon energy excitation down to ~2.2 eV for the lowest excitation, as a result of excitation energy-induced QD size selection. The observed spectral shift results from a combination of size dependencies of bandgap energy, absorption cross-section and radiative rate. The optical density of the sample shows a gradual increase for higher photon energies (Figure 1c, grey). While the fast PL lifetime cannot be explained using existing excitonic models, both spectral features—the broad tunability of the PL spectrum and the optical density characteristic for band-to-band transitions in semiconductor—are typical for an ensemble of QDs with broad size distribution and suggest excitonic origin of PL.

Another demonstration for the excitonic origin of the PL band was obtained by single QD spectroscopy performed on the synthesized materials (for more details, see Supplementary Information and Ref. 22). These investigations revealed characteristic single Si-QDs PL spectra with phonon replicas which could be related to vibration of covalent Si–C bonds on the Si-QDs surface. Single Si-QDs show spectral shifting, characteristic intermittency, negligible bleaching and the same effective PL lifetime as that of the Si-QDs ensemble reported here, thus are fully consistent with the PL results shown in Figure 1.

In order to conclude that the PL displayed in Figure 1 originates from excitons recombining at QD core-related levels, we explored the possibility of replacing the C-termination by oxygen, by which the system transforms into the well-known and thoroughly characterized O-terminated Si-QDs. This is achieved by exposure of butyl-terminated Si-QDs (PL spectrum and decay from Figure 1 shown by the green line in Figure 2a and 2b, respectively) to oxygen under intense illumination with a pulsed UV laser beam (E_{exc}=4.4 eV) with Gaussian intensity profile for different durations of time. Within 30 min, the intensity of the originally blue-green band decreases and another PL band appears in the red, around ~1.85 eV (Figure 2a, orange line). Spectral position and lifetime $\tau_{PL}\approx12$ μs (Figure 2b, red line) of this red band are characteristic for O-passivated Si-QDs of this size.[23] The red band is particularly known to dominate for smaller (about 2–3 nm) O-terminated Si-QDs, where efficient ultrafast trapping of excited carriers on surface states disables recombination of excitons from QD core-related states[5,24] (see Figure 2c for schematic illustration). When the oxidation procedure is extended for another 30 min, the intensity of the red emission at $E_{PL}\approx1.85$ eV increases even more, accompanied by further decrease of the blue-green band (Figure 2a, red line). The remaining blue-green band originates from non-oxidized Si-QDs within the low-intensity edges of the excitation/oxidation laser beam, observable by eye as a bluish halo to the brightly red emitting spot in the centre (see sketch in Figure 2a). This experiment demonstrates then that the QD surface termination can be altered *via* very simple procedure, by which spectral and temporal characteristics of emission can be very easily effectively adjusted. In the past, the reverse possibility of converting O- into C-termination (e.g., alkyl-capping) has been demonstrated for differently prepared Si-QDs.[11,20] Therefore, the present result provides the most direct evidence that the observed blue-green fast emission appears due to excitonic recombination in the Si-QDs, rather than from possible residue products in the solvent. Also absence of the red band in the original blue-green PL spectrum illustrates that the alkyl-terminated Si-QDs were not oxidized during or after the synthesis.

As clear from the above, our experimental findings prove beyond reasonable doubt that the fast blue-green PL arises due to band-to-band recombination of electrons and holes confined in the Si-QD core, and that Si-QD emission can be drastically changed by different surface terminations. In order to justify the nanosecond decay and the spectral profile of the PL signal, we have conducted theoretical modeling of the optical bandgap (Figure 3b) and radiative rate (Figure 3d) of CH_3-terminated Si-QDs of sizes between 1.8 and 4 nm. This has been done using an $sp^3d^5s^*$ empirical tight binding technique with the nearest neighbor interactions (for details, see Supplementary Information).

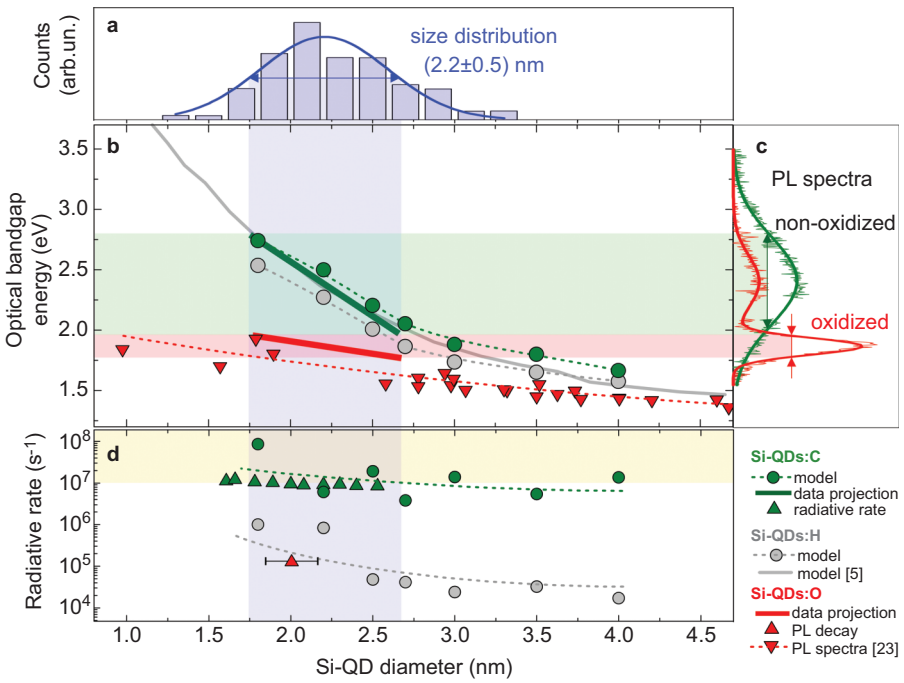

Figure 3 Comparison of the experimental results with the theoretical modeling. (**a**) Size distribution of CH_3-terminated Si-QDs, obtained from HRTEM measurements. (**b**) Tight-binding simulation of the optical band-gap in H- (grey dots) and CH_3-terminated (green dots) Si-QDs, compared with theoretically obtained optical bandgap for H-terminated Si-QDs adapted from Ref. 5 (grey line), and experimental results of optical bandgap in oxidized Si-QDs adapted from Ref. 23 (red triangles). Dashed lines are guide to the eye. The thick green and red lines depict 'cross-section' of the experimental results—size distribution (blue-shaded area), alkyl-terminated Si-QDs PL spectrum (green-shaded area) and red PL band from oxidized Si-QDs (red-shaded area). (**c**) PL emission peaks from Figure 2a for the alkyl-terminated (green) and oxidized Si-QDs (red). (**d**) Radiative recombination rates calculated by tight-binding technique for H- (grey dots) and CH_3-terminated (green dots) Si-QDs (dashed lines are guide to the eye). For comparison, the experimentally measured radiative rates for alkyl-terminated Si-QDs are shown (green triangles), together with PL lifetime of oxidized Si-QDs (red triangles). Orange-shaded area depicts range of radiative rates typical for direct bandgap materials. HRTEM, high-resolution transmission electron microscopy; PL, photoluminescence; QD, quantum dot.

Figure 3b shows Si-QD size dependence of the optical bandgap. For H-terminated Si-QDs, our model (grey dots) is in excellent agreement with previous reports (Ref. 5—grey line). For C-terminated Si-QDs, the simulation reveals that the QD-size dependence of optical bandgap (green dots) is practically identical as for H-terminated Si-QDs, evidencing that the energy of the optical bandgap of Si-QDs is only marginally influenced by the C-termination. This conclusion agrees with the findings obtained by ab-initio calculations for ultrasmall C-terminated clusters.[19] Our calculations also correlate very well with the experiment: there is an excellent agreement between the model (green dots) and the cross-section (thick green line) of the full width at half-maximum range of the experimentally measured PL spectrum (green-shaded area, based on Figures 2a and 3c—green lines) and the full width at half-maximum of the QD size distribution (blue-shaded area, based on Figure 3a), obtained from transmission electron microscopy measurements. Concomitantly, the cross-section (thick red line) for the QD size distribution (blue-shaded area) within range of the red PL band for the oxidized QDs (red-shaded area, based on Figures 2a and 3c—red line) agrees well with the size-dependence trend found experimentally for O-passivated Si-QDs (Ref. 23—red triangles). The slightly blue-shifted position of this cross-section area with respect to the experimental trend could be an indication of a small decrease in core diameter during the photo-oxidation. The weak size dependence of this O-related defect emission also suggests that the red emission band should be much narrower than the original excitonic blue-green emission band, again in an excellent agreement with the experimental findings. In this way, the QD surface oxidation scenario and the QD size tunability of the PL for the C-terminated QDs are fully confirmed. Interestingly, the spectral width of the red emission band is much narrower than usually observed for samples prepared by other techniques, such as electrochemical etching, ion implantation, sputtering or plasma synthesis (see e.g., Refs. 25–27 for the typical size broadening). This demonstrates that the size distribution of Si-QDs prepared by chemical synthesis can be better controlled, illustrating directly yet another advantage of this approach.

Figure 3d shows the radiative rates calculated for transitions between the highest valence and the lowest conduction band state (HOMO–LUMO transition) in H-terminated Si-QDs (grey dots) and CH_3-terminated Si-QDs (green dots) in ethanol for sizes between 1.8 and 4 nm. Orange-shaded area depicts the range of radiative rates typical for direct bandgap materials, such as CdSe, PbSe or GaAs. For CH_3-terminated Si-QDs, direct bandgap-like radiative rates of $k_{rad} \approx 10^7$–10^8 s^{-1} are found, whereas for H-terminated Si-QDs, the rates are $k_{rad} \approx 10^4$–10^6 s^{-1}, in agreement with previous estimations by other approaches.[2,3,6] In order to experimentally verify this theoretical result, the lower limit for the radiative rates has been estimated from the effective PL lifetime τ_{eff} and the absolute external quantum efficiency η_{ext}, *via* relation $k_{rad}(d_{QD}) \approx \eta_{ext}/\tau_{eff}(d_{QD})$ (for details, see Supplementary Information). The absolute quantum efficiency has been measured using an integration sphere technique, following the method described in Refs. 27 and 28. Using the experimentally obtained values $\tau_{eff} \approx 3$–4 ns and $\eta_{ext} \approx 4\%$, we arrive to $k_{rad} \approx 10^7$ s^{-1} (Figure 3d, green triangles). Evidently, this value is in an excellent agreement with the tight-binding simulations (green dots). For

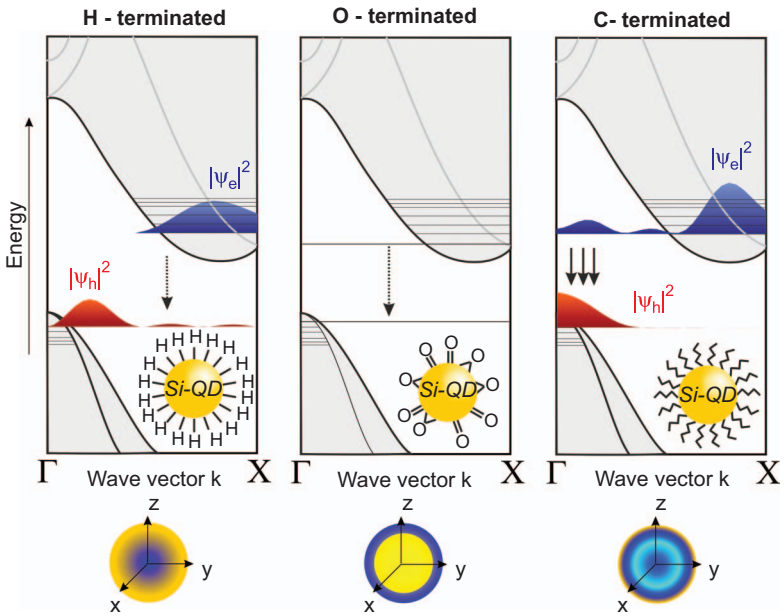

Figure 4 Schematic illustration of the dominant radiative channels in (from left to right) H-, O- and C-terminated Si-QDs. Hole and electron density in **k**-space $|\Psi(K)|^2$ in the lowest excited state for Γ–X directions are depicted in red and blue, respectively. For clarity, the wavefunctions are projected onto the bulk Si indirect bandgap structure. Below each panel, a schematic illustration of the electron density in the lowest excited state in Si-QD in the real space is given. In H-terminated Si-QDs, slow radiative rate PL originates from phonon-assisted quasi-direct excitonic recombination. In O-terminated Si QDs, slow PL is O-defect-related (adapted from model in Ref. 5). In C-terminated Si-QDs, radiative rate is dramatically enhanced as a result of direct phonon-less character of the recombination. In real space, electron density for C-terminated Si-QDs is more homogeneously distributed through the QD (for details, see Supplementary Fig. S5), when compared with H-terminated Si-QDs. In O-terminated Si-QDs, electron (and hole) is considered trapped on O-related defect state, following model in Ref. 5. PL, photoluminescence; QD, quantum dot.

comparison, we also added the PL lifetime data, as measured for the oxidized Si-QDs (red triangle).

The fast radiative rates of excitonic recombination in C-terminated QDs can be explained in terms of distribution of the electron and hole densities $|\Psi|^2$ in the lowest excited state in the real and the **k**-space (Figure 4 and Supplementary Fig. S5). Strong sensitivity to the surface modification is a typical feature of covalent semiconductors, like Si.[29] According to our tight-binding simulations, the presence of alkyl chains leads to the increased confinement of the electrons at the QD surface, since the diagonal energies of carbon atoms are smaller than those of Si atoms, by approximately 3 eV (for details, see Supplementary Information). Stronger surface confinement broadens the **k**-space distribution of the wavefunction, so that the electron density in the lowest excited state (corresponding in bulk Si to the state positioned in the Δ valley in **k**-space, close to the X-point) extends up to the Γ-point (Figure 4, right upper panel). Consequently, the probability of radiative no-phonon transitions grows as compared to both H-terminated Si-QDs (left upper panel), where electron and hole have different positions in **k**-space, rendering radiative recombination to be phonon-assisted, and O-terminated Si-QDs (Figure 4, middle upper panel) where electron-hole recombination involves O-related defect centres. In particular, the overlap between electron and hole densities along Γ–X direction only (left and right upper panels of Figure 4) is about six times larger in CH_3-terminated Si-QDs than in H-terminated ones, reflecting the direct bandgap-like character of the transition. Full tight-binding calculation provides even larger enhancement: the calculated coordinate matrix element $<h|x|e>$ between the lowest confined states equals to $\sim 10^{-10}$ cm for H-terminated Si-QDs and $\sim 30\times 10^{-10}$ cm for CH_3-terminated Si-QDs. In view of past reports on fast emission in Si-QDs, it should be noted that this situation is very different from the frequently invoked bulk-like Γ–Γ recombination from hot carrier states in oxidized Si-QDs[26] and for alkyl-capped Si-QDs.[30]

In addition to the increased radiative rates, our calculations predict also enhancement of the band-edge absorption cross-section, when compared to H- and O-terminated Si-QDs (Supplementary Fig. S6). Since this concerns the low photon energy 'solar spectrum' range, these Si-QDs might be attractive for applications in photovoltaics. Interestingly, despite dramatic enhancement in radiative rate and absorption cross-section near the band-edge, absorption spectrum profile at the band-edge remains featureless (Figure 1c), in contrast to typical direct bandgap materials such as CdSe, GaAs or PbSe. This probably results from the size dispersion and also from the relatively low density of the 'direct bandgap-like' states (Supplementary Fig. S7), when compared to typical direct bandgap materials.

CONCLUSIONS

We demonstrate a direct bandgap variant of Si-QDs—material with broadly tunable excitonic emission in the visible range, with the radiative rate enhanced about 10^2–10^3 times when compared to the smallest H- or O-terminated Si-QDs, and about 10^5 times compared to bulk Si. In particular, using optical spectroscopy of the state-of-the-art synthesized alkyl-terminated Si-QDs and theoretical modelling, we show that C-linked molecules cause dramatic modification of the Si-QD energy structure, leading to phonon-less character of excitonic recombination close to band edges. We confirm our conclusions by demonstrating that replacing C- by O-termination leads to the well-known slow red emission, with about 10^3 times lower radiative rate.

AUTHOR CONTRIBUTIONS

KD and TG conceived and designed the experiments. KD performed the experiments and analyzed the data. ANP and AAP performed the

theoretical calculations. CPU, JMJ and HZ prepared the samples. KD, WDAM de B and TG co-wrote the paper. All the authors discussed the results.

ACKNOWLEDGMENTS

This work was financially supported by Stichting der Fundamenteel Onderzoek der Materie and Stichting voor de Technische Wetenschappen. Part of this work (CPU, JMJP and HZ) was financed by the Dutch Polymer Institute for funding of UC in Functional Polymer Systems project no. 681, and (ANP and AAP) Russian Foundation for Basic Research and 'Dynasty'-Foundation of International Center for Fundamental Physics in Moscow. Authors greatly acknowledge Irina Yassievich for fruitful discussions, Loes Ruizendaal for assistance with sample preparation and H Zhang for assistance with time-resolved ultrafast spectroscopy. The photograph in Figure 1a has been provided by M T Trinh.

1 Delley B, Steigmeier EF. Quantum confinement in Si nanocrystals. *Phys Rev B* 1993; **47**: 1397.
2 Hybertsen MS. Absorption and emission of light in nanoscale silicon structures. *Phys Rev Lett* 1994; **72**: 1514–1517.
3 Belyakov VA, Burdov VA, Lockwood R, Meldrum A. Silicon nanocrystals: fundamental theory and implications for stimulated emission. *Adv Opt Technol* 2008; 279502.
4 Kovalev D, Heckler H, Polisski G, Koch F. Optical properties of Si nanocrystals. *Phys Status Solidi B* 1999; **215**: 871–932.
5 Wolkin MV, Jorne J, Fauchet PM, Allan G, Delerue C. Electronic states and luminescence in porous silicon quantum dots: the role of oxygen. *Phys Rev Lett* 1999; **82**: 197–200.
6 Goller B, Polisski S, Wiggers H, Kovalev D. Freestanding spherical silicon nanocrystals: a model system for studying confined excitons. *Appl Phys Lett* 2010; **97**: 041110.
7 Dohnalová K, Kůsová K, Pelant I. Time-resolved photoluminescence study on initial phase oxidation of small silicon nanocrystals. *Appl Phys Lett* 2009; **94**: 211903.
8 Veinot JC. Synthesis, surface functionalization, and properties of freestanding silicon nanocrystals. *Chem Commun* 2006; **40**: 4160.
9 Zou J, Kauzlarich SM. Functionalization of silicon nanoparticles *via* silanization: alkyl, halide and ester. *J Clust Sci* 2008; **19**: 341–355.
10 Ruizendaal L, Pujari SP, Gevaerts V, Paulusse JM, Zuilhof H. Bio- functional silicon nanoparticles *via* thiolene click chemistry. *Chem Asian J* 2011; **6**: 2776–2786.
11 Hessel CM, Rasch MR, Hueso JL, Goodfellow BW, Akhavan VA *et al*. Synthesis of ligand stabilized silicon nanocrystals with size-dependent photoluminescence spanning visible to near-infrared wavelengths. *Chem Mater* 2012; **24**: 393–401.
12 Rosso-Vasic M, Spruijt E, van Lagen B, de Cola L, Zuilhof H. Alkyl-functionalized oxide-free silicon nanoparticles: synthesis and optical properties. *Small* 2008; **4**: 1835–1841.
13 English DS, Pell LE, Yu Z, Barbara PF, Korgel BA. Size tunable visible luminescence from individual organic monolayer stabilized silicon nanocrystal quantum dots. *Nano Lett* 2002; **2**: 681–685.
14 Wilcoxon JP, Samara GA, Provencio PN. Optical and electronic properties of Si nanoclusters synthesized in inverse micelles. *Phys Rev B* 1999; **60**: 2704–2714.
15 Zou J, Baldwin RK, Pettigrew KA, Kauzlarich SM. Solution synthesis of ultrastable luminescent siloxane-coated silicon nanoparticles. *Nano Lett* 2004; **4**: 1181–1186.
16 Warner JH, Hoshino A, Yamamoto K, Tilley RD. Water-soluble photoluminescent silicon quantum dots. *Angew Chem Int Ed* 2005; **44**: 4550–4554.
17 Kurumoto N, Yamada T, Uchino T. Enhanced blue photoluminescence from $SiCl_4$-treated nanometer-sized silica particles. *J Non-Cryst Sol* 2007; **353**: 684–686.
18 Erratum for publication [12], published in Small. 2009; **5**: n/a.
19 Reboredo FA, Galli G. Theory of alkyl-terminated silicon quantum dots. *J Phys Chem B* 2005; **109**: 1072–1078.
20 Kůsová K, Cibulka O, Dohnalová K, Pelant I, Valenta J *et al*. Brightly luminescent organically capped silicon nanocrystals fabricated at room temperature and atmospheric pressure. *ACS Nano* 2010; **4**: 4495–4504.
21 Yang CS, Bley RA, Kauzlarich SM, Lee HW, Delgado GR. Synthesis of alkyl-terminated silicon nanoclusters by a solution route. *J Am Chem Soc* 1999; **121**: 5191–5195.
22 Dohnalová K, Fučíková A, Umesh CP, Humpolíčková J, Paulusse JM *et al*. Microscopic origin of the fast blue-green luminescence of chemically synthesized non-oxidized silicon quantum dots. *Small* 2012; **8**: 3185–3191.
23 Takeoka S, Fujii M, Hayashi S. Size-dependent photoluminescence from surface-oxidized Si nanocrystals in a weak confinement regime. *Phys Rev B* 2000; **62**: 16820–16825.
24 Godefroo S, Hayne M, Jivanescu M, Stesmans A, Zacharias M *et al*. Classification and control of the origin of photoluminescence from Si nanocrystals. *Nat Nanotechnol* 2008; **3**: 174.
25 Heitmann J, Müller F, Zacharias M, Gösele U. Silicon nanocrystals: size matters. *Adv Mater* 2005; **17**: 795.
26 de Boer WD, Timmerman D, Dohnalova K, Yassievich IN, Zhang H *et al*. Red spectral shift and enhanced quantum efficiency in phonon-free photoluminescence from silicon nanocrystals. *Nat Nanotechnol* 2010; **5**: 878–884.
27 Timmerman D, Valenta J, Dohnalová K, de Boer WD, Gregorkiewicz T. Step-like enhancement of luminescence quantum yield of silicon nanocrystals. *Nat Nanotechnol* 2011; **6**: 710–713.
28 Mangolini L, Jurbergs D, Rogojina E, Kortshagen U. Plasma synthesis and liquid-phase surface passivation of brightly luminescent Si nanocrystals. *J Lumin* 2006; **121**: 327–334.
29 Delerue C, Lannoo M. *Nanostructures: theory and modelling*. Berlin: Springer-Verlag, 2004.
30 Wilcoxon JP, Samara GA. Tailorable, visible light emission from silicon nanocrystals. *Appl Phys Lett* 1999; **74**: 3164–3166.

Supplementary Information for this article can be found on *Light: Science & Applications*' website (http://www.nature.com/lsa/)